# Learning Generalized Diffusions using an Energetic Variational Approach

Yubin Lu[1], Xiaofan Li[*1], Chun Liu[1], Qi Tang[2] and Yiwei Wang[3]

[1]*Department of Applied Mathematics, Illinois Institute of Technology, Chicago, IL 60616 United States*
[2]*School of Computational Science and Engineering, Georgia Institute of Technology, Atlanta, GA 30332 United States*
[3]*Department of Mathematics University of California Riverside, Riverside, CA 92521 United States*

December 9, 2024

**Abstract**

Extracting governing physical laws from computational or experimental data is crucial across various fields such as fluid dynamics and plasma physics. Many of those physical laws are dissipative due to fluid viscosity or plasma collisions. For such a dissipative physical system, we propose two distinct methods to learn the corresponding laws of the systems based on their energy-dissipation laws, assuming either continuous data (probability density) or discrete data (particles) are available. Our methods offer several key advantages, including their robustness to corrupted observations, their easy extension to more complex physical systems, and the potential to address higher-dimensional systems. We validate our approach through representative numerical examples and carefully investigate the impacts of data quantity and data property on the model discovery.

## 1 Introduction

Constructing surrogate models and discovering physical laws, often represented by nonlinear partial differential equations (PDEs), are two major data-driven approaches that can help us better understand complex natural phenomena. One of the most widely used methods for discovering physical laws is the physics-informed neural network (PINN) [48]. The idea of PINN is to train neural networks using a loss function based on the underlying partial differential equation and noisy observation data. This approach can be traced back to at least the works in [50, 1, 18]. Another powerful approach for extracting governing physical laws from data is a sparse identification of nonlinear dynamical systems (SINDy) [5]. SINDy has gained popularity due to its interpretability and computational efficiency. The SINDy framework is motivated by the pioneer work [4, 53], which uses symbolic regression to recover physical equations from data. Later, a weak-form version of SINDy was developed for learning PDEs [39, 38] and extended to cover mean-field equations [40] and Hamiltonian systems [41]. Koopman operator theory is also used to establish various data-driven analysis for complex dynamics [6, 59, 28]. Nonparametric regression techniques for learning interaction kernels [34, 32, 29, 15, 42, 33, 14] are developed for various equations. Flow maps [10, 12, 31] and kernel flows [60] for learning dynamical systems are introduced. Probabilistic/statistical methods,

[*]Corresponding author: lix@iit.edu

1

including Bayesian inferences, maximum likelihood methods, and Wasserstein distances, are introduced to learn stochastic dynamical systems [13, 45, 36]. More recently, in order to maintain the physical properties (e.g., invariant quantities for conserved systems or dissipation rates for dissipative systems) of the original system while learning the system, various structure-preserving learning strategies are developed to learn Hamiltonian systems [27, 7, 8, 37, 3, 16, 19, 23, 11, 30], energy dissipative systems [62, 61, 25], and, more generally, metriplectic systems [20, 21].

However, most of the existing work establish the learning framework based on the corresponding equations, such as (stochastic) ordinary differential equations (SDE/ODE for short) and PDEs. The learned models may not preserve the fundamental physical law of dissipation. Recently, there are growing interesting of learning thermodynamically consistent physical model from variational principles, such as General Equation for Non-Equilibrium Reversible-Irreversible Coupling (GENERIC) formalism [22, 64] and Onsager principle [26, 61]. These variational principles model complex physical processes by accounting for both energy conservation (in reversible processes) and energy dissipation (in irreversible processes). The key idea behind these variational principle-based learning approaches is to parameterize the physical quantities using neural networks while constructing loss functions based on equations derived from these principles.

The goal of this work is to propose a new learning framework based on the energy-dissipation laws of the target physical systems, without relying on the governing equations. Our proposed methods offer several benefits, including robustness to corrupted observations, easy extensions to more general physical systems, and has the potential to handle higher dimensional systems. In this work, we focus on learning potential function and noise intensity in one-dimensional generalized diffusion to illustrate our method and explore its performance under different settings. Extending the approach to higher-dimensional problems and other physical systems is straightforward. For much higher dimensional problems, we leave this as future work.

The rest of the paper is organized as follows. Section 2 provides a brief introduction to the energetic variational approach for generalized diffusions. In Section 3, we propose two methods for learning the governing laws of the systems based on their energy-dissipation laws, using either continuous data (probability density) or discrete data (SDE particles). Section 4 presents several representative examples to validate the performance of our methods. Finally, we conclude with a brief discussion and propose an alternative approach for learning the system based on another type of discrete data (ODE particles) in Section 5.

## 2    Formulation

Before proposing the learning framework, we briefly introduce the energetic variational approach (EnVarA for short) [17] for generalized diffusions, which plays an important role in our proposed learning frameworks in the next section.

Motivated by non-equilibrium thermodynamics, particularly the seminal work of Rayleigh [55] and Onsager [43, 44], a complex system can be described by an energy-dissipation law

$$\frac{d}{dt}E^{\text{total}} = -\Delta \leq 0, \tag{1}$$

where $E^{\text{total}}$ is the sum of the kinetic energy $\mathcal{K}$ and the Helmholtz free energy $\mathcal{F}$, and $\Delta$ is the rate of energy dissipation. Based on the energy-dissipation law (1), EnVarA is a unique, well-defined way to derive the dynamics of the underlying system using the least action principle (LAP) and the maximum dissipation principle (MDP). To be more specific, for the Hamiltonian part of the system, one can employ the LAP, taking variation of the action functional $\mathcal{A}(\boldsymbol{x}) = \int_0^T (\mathcal{K} - \mathcal{F}) \, \mathrm{d}t$

with respect to $\boldsymbol{x}$ (the trajectory in Lagrangian coordinates) [17, 2], to derive the conservative force, i.e., $\delta\mathcal{A} = \int_0^T \int_\Omega (\text{force}_{\text{iner}} - \text{force}_{\text{conv}}) \cdot \delta\boldsymbol{x} \, \mathrm{d}\boldsymbol{x}\mathrm{d}t$. For the dissipation part, one can apply the MDP, taking the variation of the Onsager dissipation functional $\mathcal{D}$ with respect to the "rate" $\boldsymbol{x}_t$, to derive the dissipative force, i.e., $\delta\mathcal{D} = \int_\Omega \text{force}_{\text{diss}} \cdot \delta\boldsymbol{x}_t \, \mathrm{d}\boldsymbol{x}$, where the dissipation functional $\mathcal{D} = \frac{1}{2}\triangle$ in the linear response regime [44]. Subsequently, the force balance condition connects the conservative force and the dissipation force providing the evolution equation of the studied system

$$\frac{\delta\mathcal{D}}{\delta\boldsymbol{x}_t} = \frac{\delta\mathcal{A}}{\delta\boldsymbol{x}}. \tag{2}$$

The EnVarA has been successfully applied to build various mathematical models in physics, chemical engineering, and biology [57, 58].

**Generalized Diffusion**  Let us consider the following random process

$$\mathrm{d}\boldsymbol{X}_t = \boldsymbol{a}(\boldsymbol{X}_t)\mathrm{d}t + \sigma(\boldsymbol{X}_t)\mathrm{d}W_t, \tag{3}$$

where $W$ is a standard $n$-dimensional Brownian motion, the state variable $\boldsymbol{X}_t$ and the drift coefficient $\boldsymbol{a}$ are two $n$-dimensional vectors, the noise intensity $\sigma$ is a scalar function, and $t \in \mathbb{R}^+ \cup \{0\}$. If the stochastic integral of (3) is interpreted as backward Itô integral, one may obtain the following Fokker-Planck equation (See (c) in Remark 2.1):

$$f_t + \nabla \cdot (\boldsymbol{a}f) = \frac{1}{2}\nabla \cdot [\sigma^2\nabla f], \tag{4}$$

where $f(\boldsymbol{x}, t)$ is the probability density function of the state variable $\boldsymbol{X}_t$.

When following the fluctuation-dissipation theorem, one restricts the convection coefficient

$$\boldsymbol{a} = -\frac{1}{2}\sigma^2\nabla\psi, \tag{5}$$

where $\psi$ is the potential function and $\sigma$ is the noise intensity.

The Fokker-Planck equations (4) with the condition (5) can be obtained from variation of the following energy dissipative law:

$$\frac{d\mathcal{F}[f]}{dt} = -\int_\Omega \frac{f}{\sigma^2/2}|\boldsymbol{u}|^2 d\boldsymbol{x}, \tag{6}$$

along with the continuity equation of the probability density

$$f_t + \nabla \cdot (f\boldsymbol{u}) = 0. \tag{7}$$

Here, $\boldsymbol{u}$ is a certain average velocity of all stochastic trajectories, and $\mathcal{F}[f]$ is the free energy is defined by

$$\mathcal{F}[f] := \int_\Omega [f \ln f + \psi f] \, d\boldsymbol{x}, \tag{8}$$

One can derive the evolution equation (4) by the general framework of EnVarA [17]. Note that

$$\mathcal{K} = 0, \qquad \mathcal{F} = \int_\Omega [f \ln f + \psi f] \, d\boldsymbol{x}, \qquad \mathcal{D} = \frac{1}{2}\int_\Omega \frac{f}{\sigma^2/2}|\boldsymbol{u}|^2 d\boldsymbol{x}. \tag{9}$$

To apply the LAP, we need first introduce the concept of flow map $\boldsymbol{x}(\boldsymbol{X}, t)$, defined through

$$\begin{cases} \frac{\mathrm{d}}{\mathrm{d}t}\boldsymbol{x}(\boldsymbol{X}, t) = \boldsymbol{u}(\boldsymbol{x}(\boldsymbol{X}, t), t), \\ \boldsymbol{x}(\boldsymbol{X}, 0) = \boldsymbol{X}. \end{cases} \tag{10}$$

3

for a given velocity field $\boldsymbol{u}$. Here $\boldsymbol{X}$ is the Lagrangian coordinate and $\boldsymbol{x}$ is the Eulerian coordinates. For fixed $\boldsymbol{X}$, $\boldsymbol{x}(\boldsymbol{X}, t)$ can be interpreted as the trajectory of the particle that is initially located at $\boldsymbol{X}$. Due to the mass conservation, $f(\boldsymbol{x}, t)$ can be viewed as the function of the flow map $x(\boldsymbol{X}, t)$, as

$$f(\boldsymbol{x}, t) = f_0(\boldsymbol{X}) / \det(\nabla_X \boldsymbol{x}(\boldsymbol{X}, t)) \tag{11}$$

where $f_0(\boldsymbol{X})$ is the initial density. Consequently, one can take the variational of the action functional with respect to the flow map $\boldsymbol{x}(\boldsymbol{X}, t)$. The final force balance equation is given by

$$\boldsymbol{u}(\boldsymbol{x}, t) = -\left( \frac{\sigma^2}{2} \nabla \ln f + \frac{\sigma^2}{2} \nabla \psi \right), \tag{12}$$

which is the velocity derived from the energy-dissipation law (6). Combining with the continuity equation $f_t + \nabla \cdot (\boldsymbol{u} f) = 0$, one can obtain the Fokker-Planck equation (4) with $\boldsymbol{a}$ given by (5). We refer the interested reader to [17, 24] and the references therein for more details.

*Remark* 2.1. There are at least three ways to express the energy-dissipation law based on different interpretations of the stochastic integral of (3). To be more specific, writing a Taylor expansion of probability distribution function $f(\boldsymbol{x}, t)$, one may obtain the following PDEs [17]:

(a) $f_t + \nabla \cdot (\boldsymbol{a} f) = \frac{1}{2} \Delta(\sigma^2 f)$ if using Itô integral,

(b) $f_t + \nabla \cdot (\boldsymbol{a} f) = \frac{1}{2} \nabla \cdot [\sigma \nabla(\sigma f)]$ if using Stratonovich integral,

(c) $f_t + \nabla \cdot (\boldsymbol{a} f) = \frac{1}{2} \nabla \cdot [\sigma^2 \nabla f]$ if using backward Itô integral, yielding PDE with self-adjoint diffusion term.

If the convection coefficient satisfies the fluctuation-dissipation theorem (5), i.e. $\boldsymbol{a} = -\frac{1}{2} \sigma^2 \nabla \psi$, then the above PDEs may be obtained from variation of the following energy laws respectively

(a) $\frac{d}{dt} \int \left[ f \ln(\frac{1}{2} \sigma^2 f) + \psi f \right] d\boldsymbol{x} = -\int \frac{f}{\sigma^2/2} |\boldsymbol{u}|^2 d\boldsymbol{x}$,

(b) $\frac{d}{dt} \int \left[ f \ln(\sigma f) + \psi f \right] d\boldsymbol{x} = -\int \frac{f}{\sigma^2/2} |\boldsymbol{u}|^2 d\boldsymbol{x}$,

(c) $\frac{d}{dt} \int \left[ f \ln f + \psi f \right] d\boldsymbol{x} = -\int \frac{f}{\sigma^2/2} |\boldsymbol{u}|^2 d\boldsymbol{x}$. along with the mass conservation:

$$f_t + \nabla \cdot (\boldsymbol{u} f) = 0. \tag{13}$$

*Remark* 2.2. In the current study, we establish the learning framework based on the expression (c) in Remark 2.1. Therefore, the SDE (3) is interpreted as a backward Itô integral correspondingly. The reason for choosing (c) is that both sides of the first two expressions, (a) and (b), depend on the noise intensity $\sigma$, which exacerbates the ill-posedness of the problem, as we must balance both sides during the training process. We need to rewrite it as an Itô SDE

$$d\boldsymbol{X}_t = \left[ \boldsymbol{a}(\boldsymbol{X}_t) + \nabla(\frac{1}{2} \sigma^2(\boldsymbol{X}_t)) \right] dt + \sigma(\boldsymbol{X}_t) dW_t$$

in order to simulate the backward Itô integral in (3) using the Euler-Maruyama scheme. It should be noted that there is a slight abuse of notation here. The stochastic integral $\sigma(\boldsymbol{X}_t) dW_t$ in this context is interpreted as an Itô integral, whereas the stochastic integral $\sigma(\boldsymbol{X}_t) dW_t$ in (3) is interpreted as a backward Itô integral.

## 3 Learning frameworks

In this section, we will propose two learning frameworks with two types of data [continuous data (probability density) or discrete data (particle)] aiming to identify (partial) dynamics of the generalized diffusion (3).

We assume that the generalized diffusion satisfies the fluctuation-dissipation theorem that tells us the relation between the noise intensity and the drift term, i.e. $\boldsymbol{a} = -\frac{1}{2}\sigma^2\nabla\psi$ in (3). Our goal is to identify the potential function $\psi$ and/or the noise intensity $\sigma^2$ of the generalized diffusion (3) from data. Moreover, we will explore the impact of data property on the learning tasks, and propose different learning frameworks to accommodate the given data.

We introduce two different ways to learn the potential function $\psi$ and/or the noise intensity $\sigma^2$ based on different training data: the density evolution generated by the Fokker-Planck equation (4), or particles generated by the stochastic differential equation (3). Both of the proposed methods are based on the energy functional (8). Thanks to the fluctuation-dissipation theorem, the system (3) or (4) satisfies the energy-dissipation law (6). Therefore, we can learn the potential function $\psi$ and/or the noise intensity $\sigma^2$ by checking against the energy-dissipation law (6).

We will construct the loss function based on the energy-dissipation law (6). Leveraging the energy-dissipation law to construct the loss function, rather than using the governing equations, offers several advantages. First, it relies solely on an energy law, bypassing the need for information from the governing equations. Second, since the energy law is expressed in an integral (weak) form, it imposes weaker regularity requirements on the density function, which is likely to be more robust to corrupted observations compared to loss functions based on governing equations. Third, the integral form of the loss function has the potential to be extended to handle higher dimensional problems efficiently, such as through the use of particle methods.

In this section the energy-dissipation law is expressed in terms of the probability density function $f$, as the most straightforward way. For simplicity, we illustrate our methods by assuming the noise intensity $\sigma^2$ is known and focus on learning the potential function $\psi$. Alternatively, we could also learn the noise intensity $\sigma^2$ while assuming the potential function $\psi$ is known. Here we let the unknown potential function $\psi(\boldsymbol{x})$ be approximated by a neural network $\psi_{nn}(\boldsymbol{x};\theta)$.

## 3.1 Density-based Method

Since the free energy $E$ and the velocity $\boldsymbol{u}$ in (8) and the dissipation rate in (6) are expressed in terms of the probability density function $f$, it is most straightforward to compute the loss function based on the density data $f$. To be specific, our training data are observation dataset (probability density function), denoted as $\{(f(\boldsymbol{x}_{i,j},t_1), f(\boldsymbol{x}_{i,j},t), f(\boldsymbol{x}_{i,j},t_2))\}_{i,j=1}^{N,M}$, where $t_1 = t - \delta t$ and $t_2 = t + \delta t$ for a given observation time step size $\delta t$, $\{\boldsymbol{x}_{i,j}\} \subset \Omega$ are the $N$ uniform mesh grid points for each $j$ with grid size $\Delta x$, and $M$ is the number of data sets which could be generated from multiple initial distributions.

The free energy (8) at time $t$ can be approximated by the following Riemann sum approximation

$$E_j^N(t,\theta) = \sum_{i=1}^{N} \left[ f(\boldsymbol{x}_{i,j},t)\ln f(\boldsymbol{x}_{i,j},t) + \psi_{nn}(\boldsymbol{x}_{i,j};\theta)f(\boldsymbol{x}_{i,j},t) \right] \Delta x. \tag{14}$$

Since the density function data is assumed to be available in this case, we construct the loss function based on the original energy-dissipation law (6)

$$\theta^* = \arg\min_{\theta} \sum_{j=1}^{M} \lambda(j) \left\| \frac{E_j^N(t_2;\theta) - E_j^N(t_1;\theta)}{t_2 - t_1} + \Delta x \sum_{i=1}^{N} \frac{f(\boldsymbol{x}_{i,j},t)}{\sigma^2/2} \left| \frac{\sigma^2}{2}\nabla\ln f(\boldsymbol{x}_{i,j},t) + \frac{\sigma^2}{2}\nabla\psi_{nn}(\boldsymbol{x}_{i,j};\theta) \right|^2 \right\|^2, \tag{15}$$

where $t_1 = t - \delta t$ and $t_2 = t + \delta t$ for a given observation time step size $\delta t$ and $\lambda$ is an user-defined weighting function. We note that, if the training data for $f$ were obtained by solving the Fokker-Planck equation (4), it would be computationally expensive in high dimensions.

*Remark* 3.1. The loss function (15) is in an integral/summation form, which has lower regularity requirements compared to the corresponding PDE (4). This integral form is expected to enhance the robustness of the proposed density-based method, particularly when the density function is not smooth enough or the observed density function is affected by polluted observations. We will present a simple comparison between our EnVarA-based method and a simplified PDE-based method in the numerical examples in the next section.

*Remark* 3.2. We can learn the potential function $\psi$ by minimizing the loss function (15) given the noise intensity $\sigma^2$. Conversely, we can also learn the noise intensity $\sigma^2$ if the potential function $\psi$ is provided. Indeed, these two learning tasks have different data requirements for the training data $\{(f(\boldsymbol{x}_{i,j}, t_1), f(\boldsymbol{x}_{i,j}, t), f(\boldsymbol{x}_{i,j}, t_2))\}_{i,j=1}^{N,M}$ in the proposed density-based method. By noticing that (15) is a weak-form loss function, the two learning problems are ill-posed in general. When learning the potential function $\psi$, if the training data are stationary, the approximation of $dE/dt$ in the loss function (15) becomes zero. As a result, the originally ill-posed problem transforms into a well-posed one, meaning that (15) serves as a point-wise loss function in this case. In contrast, stationary training data are not suitable for learning the noise intensity $\sigma^2$, since the approximation of $dE/dt$ remains zero, making zero a minimizer of the loss function. We will further explore this in the next section through numerical examples.

*Remark* 3.3. The free energy of the system (3) exponentially over time, particularly in the initial stage, the derivative $(dE/dt)$ is large. We found first-order schemes lack sufficient accuracy, which significantly impacts the performance of our method. Therefore, we use a second-order scheme here instead of the forward Euler scheme to achieve more accurate derivative $(dE/dt)$ estimates. To do so, we collect training data $\{(f(\boldsymbol{x}_{i,j}, t_1), f(\boldsymbol{x}_{i,j}, t), f(\boldsymbol{x}_{i,j}, t_2))\}_{i,j=1}^{N,M}$ at three time instances to compute the derivative $dE/dt$ using a more accurate finite difference scheme, specifically a second-order central difference approximation.

## 3.2 Particle-to-density method

Next, we consider the case where the probability function $f$ corresponding to the state variable is not readily available. Solving a high-dimensional Fokker-Planck equation using a continuous representation of $f$ faces the curse of dimensionality, which becomes less practical. Therefore, we propose an alternative way to establish the learning framework here.

Suppose that we can access particle data that satisfy the SDE (3) instead of the probability density function $f$. The observation dataset (particles) is denoted by $\{(\boldsymbol{x}_{i,j}(t_1), \boldsymbol{x}_{i,j}(t), \boldsymbol{x}_{i,j}(t_2))\}_{i,j=1}^{N,M}$. The number $N$ here is the sample size of a distribution function opposed to the numbers of grid points in the density-based method proposed in the previous subsection. One can approximate the probability density function $f$ using particle data $\{(\boldsymbol{x}_{i,j}(t_1), \boldsymbol{x}_{i,j}(t), \boldsymbol{x}_{i,j}(t_2))\}_{i,j=1}^{N,M}$, denoted by $f_N$, so that the loss function (15) can be computed as in the density-based method. In this work, we consider only 1D cases. We use the kernel density estimation method [51, 47] to approximate the density function. For higher-dimensional systems, one can employ more efficient methods to approximate the density function such as normalizing flows [49, 46, 35]. Subsequently, the loss function for the particle-to-density method can be obtained by replacing $f$ with $f_N$ in the loss function (15) of the density-based method

$$\theta^* = \arg\min_\theta \sum_{j=1}^M \lambda(j) \left\| \frac{E_j^N(t_2;\theta) - E_j^N(t_1;\theta)}{t_2 - t_1} + \Delta x \sum_{i=1}^N \frac{f_N(\boldsymbol{x}_{i,j}, t)}{\sigma^2/2} \left| \frac{\sigma^2}{2} \nabla \ln f_N(\boldsymbol{x}_{i,j}, t) + \frac{\sigma^2}{2} \nabla \psi_{nn}(\boldsymbol{x}_{i,j}; \theta) \right|^2 \right\|^2,$$

(16)

where the energy is

$$E_j^N(t, \theta) = \sum_{i=1}^N \left[ f_N(\boldsymbol{x}_{i,j}, t) \ln f_N(\boldsymbol{x}_{i,j}, t) + \psi_{nn}(\boldsymbol{x}_{i,j}; \theta) f_N(\boldsymbol{x}_{i,j}, t) \right] \Delta x.$$

(17)

Compared with the density-based method, the particle-to-density method gives a less accurate learning framework since we need to approximate the density function using particle data. However, as a reward at the cost of losing accuracy, we can obtain training datasets efficiently, especially in high dimensions, since we can solve the SDE (3) instead of solving the Fokker-Planck equation (4).

## 4    Numerical Examples

In this section, we will investigate the performance of the three learning frameworks proposed in the previous section (i.e., the density-based method and the SDE particle-based method) under different settings. Furthermore, we will explore the impacts of data quality and quantity on the learning results.

For all examples, we use a constant weighting function $\lambda \equiv 1$ in the loss functions (15) and (16). For training, we employ a fully-connected neural network with one hidden layer and 32 nodes per layer. The activation function is **Tanh()**, and we use **Adam** as the optimizer with a learning rate $5 \times 10^{-4}$. The neural network is trained for 20000 epochs with the batch size 5 (20 groups data) in most of the examples, unless otherwise specified. In the particle-to-density case, we generate $5 \times 10^4$ samples as training data when using the particle-to-density method.

In what follows, we consider the SDE (3), i.e. $d\boldsymbol{X}_t = \boldsymbol{a}(\boldsymbol{X}_t)dt + \sigma(\boldsymbol{X}_t)dW_t$, where the drift term $\boldsymbol{a}$ satisfies the fluctuation-dissipation theorem $\boldsymbol{a} = -\frac{1}{2}\sigma^2\nabla\psi$. Our goal is to identify the potential function $\psi$ or the noise intensity $\sigma^2$ and the ground truth potential function $\psi$ and noise intensity $\sigma^2$ will be specified in each example. It should be noted that the learned potential function can be shifted in the $y$-direction, as adding a constant to the potential function does not affect the system's evolution.

### 4.1    Learning potential function

In this subsection, we study the performance of the density-based and particle-to-density methods for learning the potential function $\psi$ using two different cases.

*Example* 4.1. We consider the potential function $\psi(x) = \frac{1}{2}x^4 - x^2$ and the noise intensity $\sigma(x) = \frac{1}{x^2+1}$. Our goal is to identify the potential function $\psi$ (in what follows, we refer to both $\sigma$ and $\sigma^2$ as noise intensity) since we cannot determine the sign of the function $\sigma$.

The training data $\{(f(x_{i,j}, t_1), f(x_{i,j}, t), f(x_{i,j}, t_2))\}_{i,j=1}^{N,M}$ are obtained by solving the Fokker-Planck equation (4) in a bounded domain $\Omega = [-3,3]$ with grid size $\Delta x = 0.01$ and time step size $\Delta t = 0.001$ or estimating the density function $f$ from the SDE (3) particles. We simulate 20 different initial distributions $\mathcal{N}(\mu, 0.2^2)$ (the mean values $\mu$ are uniformly spaced in domain $[-2, 2]$) and choose the snapshots at $t_1 = 2.495$, $t = 2.5$ and $t_2 = 2.505$ as our training data (so the observation time step size is $\delta t = 5\Delta t$ where $\Delta t$ is the time step used in the Fokker-Planck solver),

i.e., the hyperparameter $M = 20$ in the loss function (15). Since the loss function (15) is in an integral form, it cannot be uniquely determined using a single group of density data ($M = 1$). Therefore, we chose to use 20 groups of data ($M = 20$) here. Figure 1a shows the learned potential function $\psi_{nn}$ together with the target $\psi$ for the given $\sigma(x) = \frac{1}{x^2+1}$. Figure 1b shows the learned potential function using the particle-to-density method. As expected, the density-based method outperforms the particle-to-density method, as the latter introduces an additional approximation error when estimating the density function. Even so, the particle-to-density method still yields good results and may be advantageous in high-dimensional problems, which we leave for future work.
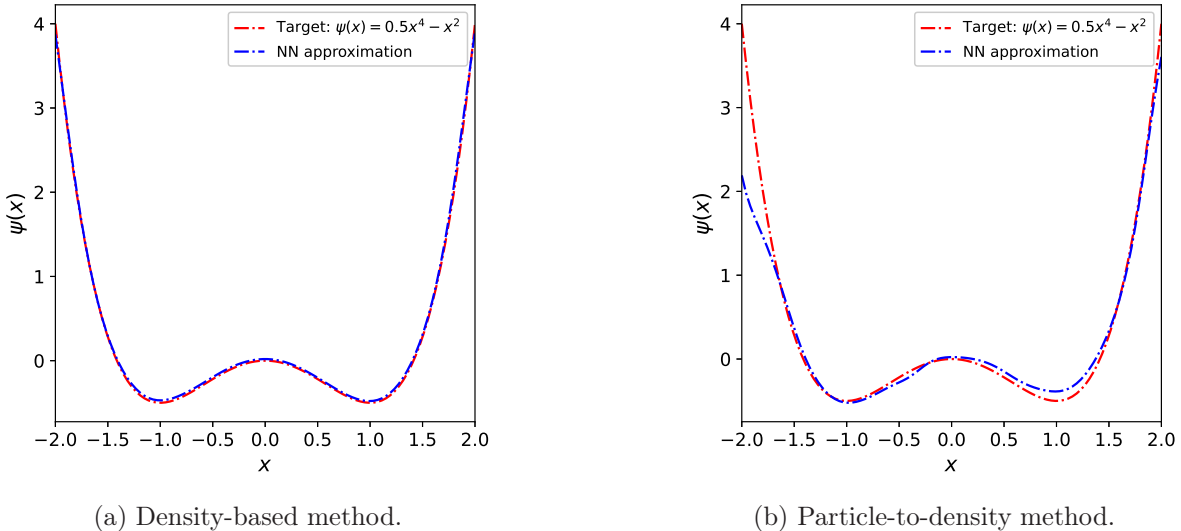


(a) Density-based method.



(b) Particle-to-density method.

Figure 1: *The learned potential function $\psi_{nn}$ (blue lines) verse the ground truth (G.T.: $\psi(x) = \frac{1}{2}x^4 - x^2$) (red lines), using the density-based method (Figures 1a) and the particle-to-density method (Figures 1b).*

*Example* 4.2. We intend to learn the potential function $\psi$ from training data with different properties. Let's revisit the energy-dissipation law (6) as follows

$$\frac{dE}{dt} = -\int_\Omega \frac{f}{\sigma^2/2}|\boldsymbol{u}|^2 d\boldsymbol{x}, \tag{18}$$

where the free energy and the velocity $\boldsymbol{u}$ are defined by

$$E[f] = \int_\Omega [f \ln f + \psi f]\, d\boldsymbol{x}, \qquad \boldsymbol{u} = -\left(\frac{\sigma^2}{2}\nabla \ln f + \frac{\sigma^2}{2}\nabla\psi\right). \tag{19}$$

The unknown function $\psi$ appears on both sides of the energy-dissipation law, leading to an inverse problem that is generally ill-posed, as one seeks to recover the potential function $\psi$ from the integral. This is the reason that, in Example 4.1, we select $M$ groups of initial data as Gaussian-type test functions trying to better determine the gradient of the potential function. However, the ill-posed problem can be avoided by using steady-state data. In the steady state, the time derivative of the energy equals zero, i.e., $\frac{dE}{dt} = 0$. Moreover, the right-hand side of the energy-dissipation law reaches its unique minimizer when the velocity $\boldsymbol{u} = 0$. Given that the noise intensity is specified and the density function $f$ corresponds to the training data, it follows that the gradient of the potential function is uniquely determined.

To illustrate this observation, we aim to learn a triple-well potential $\psi$ using the training data at different time instances, with the noise intensity $\sigma^2(x) = \left[1 + \frac{1}{2}\cos(3x + \frac{1}{2})\right]^2$ provided.

The training data are obtained by solving the Fokker-Planck equation (4) using a similar setting of the previous example and the observation time step size is still chosen as $\delta t = 5\Delta t$. Figure 2a shows the evolution of the free energy. Figure 2b shows the learned triple-well potential using data from 20 groups at time $t = 20$ (unsteady state in this case), while Figure 2c shows the learned triple-well potential using data from 1 group at time $t = 200$ (steady state). For the latter, we trained for 50000 epochs due to the limited data (1 group), compared to the former, which used data from 20 groups. As we can see, both sets of training data are able to learn the triple-well potential, but the latter is more accurate than the former because it avoids the ill-posedness problem.
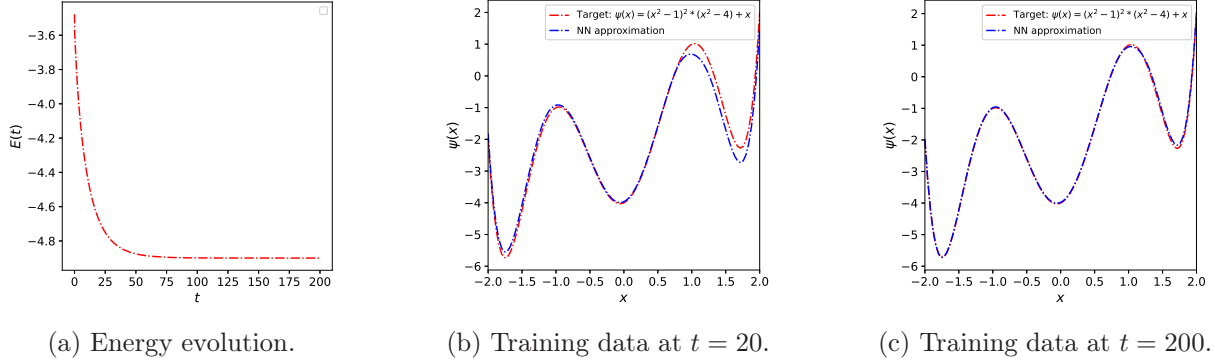


(a) Energy evolution.    (b) Training data at $t = 20$.    (c) Training data at $t = 200$.

Figure 2: *(a) The evolution of the energy $E(t)$ for the true density $f$ with $\psi(x) = (x^2-1)^2(x^2-4)+x$ and $\sigma^2(x) = \left[1 + \frac{1}{2}\cos(3x + \frac{1}{2})\right]^2$. The learned potential function $\psi_{nn}$ (blue) compared with the G.T. (red) using the density-based method for training data at (b) $t = 20$ (unsteady) and (c) $t = 200$ (steady state).*

## 4.2   Learning noise intensity

In this subsection, we validate the performance of the density-based and particle-to-density methods for learning the noise intensity $\sigma^2$ using three different cases.

*Example* 4.3. We consider the potential function $\psi(x) = \frac{1}{2}x^4 - x^2$ and the noise intensity $\sigma(x) = \frac{1}{x^2+1}$. The settings of this example are almost the same as in Example 4.1, except that we aim to learn the noise intensity $\sigma^2$ instead of the potential function $\psi$. Figure 3a shows the learned noise intensity $\sigma^2_{nn}$ for the given potential $\psi(x) = \frac{1}{2}x^4 - x^2$ along with the target $\sigma^2(x) = \frac{1}{(x^2+1)^2}$ using the density-based method.

The training data $\{(f(x_{i,j}, t_1), f(x_{i,j}, t), f(x_{i,j}, t_2))\}_{i,j=1}^{N,M}$ are obtained by solving the Fokker-Planck equation (4) in a bounded domain $\Omega = [-3,3]$ with grid size $\Delta x = 0.01$ and time step size $\Delta t = 0.001$ or estimating the density function $f$ from the SDE (3) particles. We simulate 20 different initial distributions of $\mathcal{N}(\mu, 0.2^2)$, where the mean values $\mu$ are uniformly spaced in domain $[-2, 2]$, and choose the snapshots at $t_1 = 0.495$, $t = 0.5$ and $t_2 = 0.505$ as our training data (so the observation time step size is $\delta t = 5\Delta t$), i.e., the hyperparameter $M = 20$ in the loss function (15). Figure 3b shows the learned noise intensity using the particle-to-density method. As in Example 4.1, the density-based method outperforms the particle-to-density method. The particle-to-density method still provides a reasonable profile of the noise intensity. For the particle-to-density method, it can be observed that the learned potential function $\psi$ in Figure 1 are more accurate than the learned noise intensity $\sigma^2$ in Figure 3. This suggests that our method may lack

9

robustness in learning the noise intensity $\sigma^2$. This is not coincidental: the issue stems from the loss function (15), as we will demonstrate with the following example.
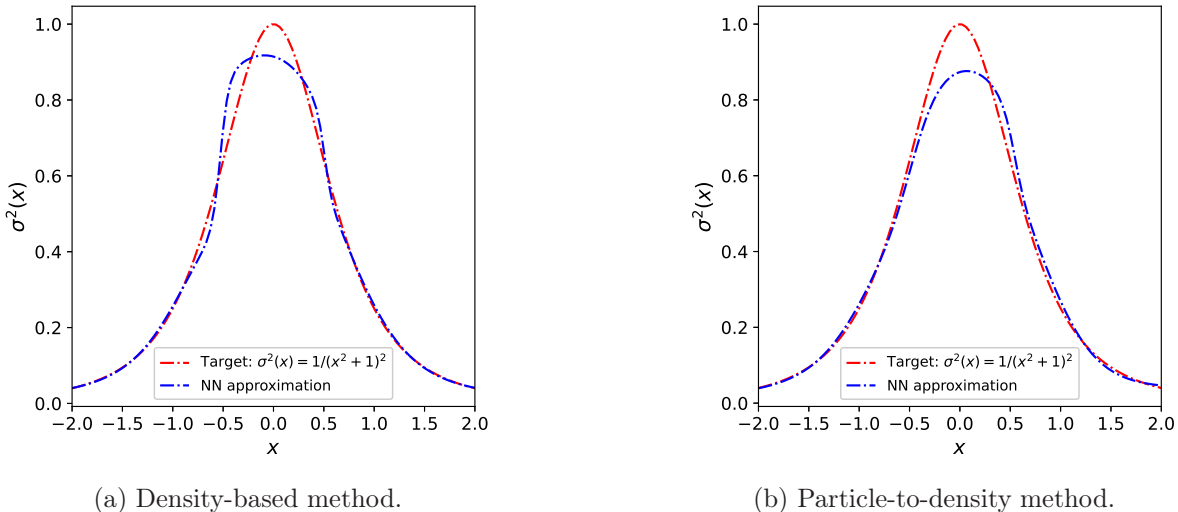


(a) Density-based method.

(b) Particle-to-density method.

Figure 3: *The learned noise intensity $\sigma^2_{nn}$ (blue lines) compared with the ground truth (G.T.: $\sigma^2(x) = \frac{1}{(x^2+1)^2}$) (red lines), using the density-based method (Figures 3a) and the particle-to-density method (Figures 3b).*

*Example* 4.4. In this example, our goal is to learn a more complicated noise intensity $\sigma^2(x) = \left[1 + \frac{1}{2}\cos(3x + \frac{1}{2})\right]^2$ using the density-based method, where the potential function $\psi(x) = \frac{1}{2}x^4 - x^2$ is given. The training data are obtained by solving the Fokker-Planck equation (4) using the same setting of the previous example and the observation time step size is still chosen as $\delta t = 5\Delta t$.

Figure 4a shows for the learned noise intensity compared with the true one. As we can see, we can only learn a rough profile of the noise intensity. The reason is that the training data are selected at the initial stage, where the approximation of the derivative $dE/dt$ is less accurate compared to data near the steady state (see Remark 3.3). Additionally, we cannot use data near the steady state to learn the noise intensity because when the system reaches steady state, the energy has already minimized, indicating that diffusion has stopped. Consequently, the energy-dissipation law no longer provides information about the noise intensity. Balancing the error in the derivative approximation with the information about the noise intensity is left for future work. Note that one can build in the periodicity strongly by learning a neural network with input of $\sin(3x)$ and $\cos(3x)$. Such an architecture improves the learning result slightly (Figure 4b), but it still does not fully resolve the challenge of balancing errors in derivative approximation with the information about noise intensity.

## 4.3 Corrupted observations

*Example* 4.5. **(Corrupted observations, EnVarA vs PDE-based method)**. In this example, we provide a simple comparison between our EnVarA-based learning framework and a PDE-based learning framework for corrupted observations aiming to show the robustness of our method. To be more specific, motivated by the PDE-based learning framework [52, 50, 1, 18], we construct the
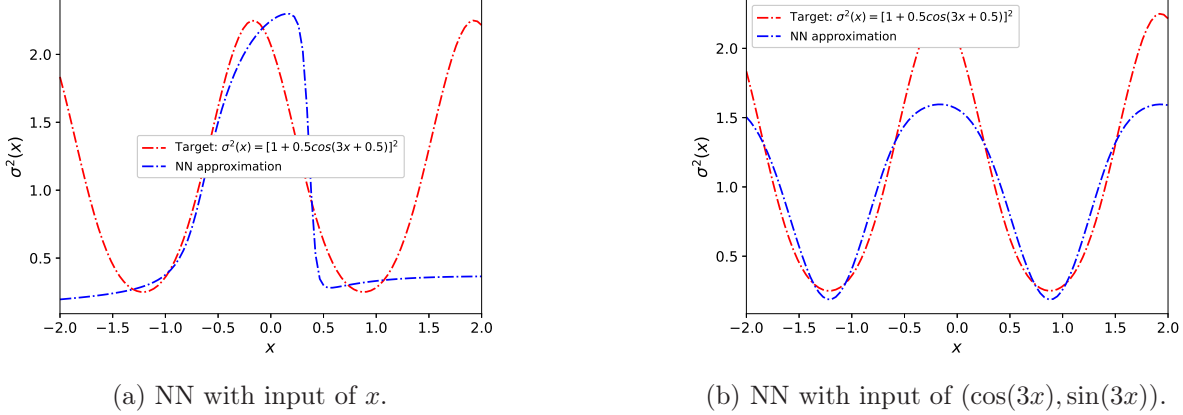
(a) NN with input of $x$.



(b) NN with input of $(\cos(3x), \sin(3x))$.

Figure 4: The learned noise intensity $\sigma^2$ (blue line) compared with the G.T. (red line) $\sigma^2(x) = \left[1 + \frac{1}{2}\cos(3x + \frac{1}{2})\right]^2$ using the density-based method. (a) Learning a neural network (NN) with input of $x$. (b) Learning a neural network with input of $(\cos(3x), \sin(3x))$.

following loss function based on the Fokker-Planck equation (4)

$$
\mathrm{L}_{\mathrm{PDE}} = \frac{1}{NM} \sum_{i,j=1}^{N,M} \left[ \frac{f_i^{j+1} - f_i^{j-1}}{2\delta t} + \nabla \cdot \left( \boldsymbol{a}_i f_i^j \right) - \frac{1}{2} \nabla \cdot \left( \sigma_i^2 \nabla f_i^j \right) \right]^2, \tag{20}
$$

where the drift term $\boldsymbol{a} = -\frac{\sigma^2}{2}\nabla\psi$, $f_i^j = f(x_i(t_j))$, $\boldsymbol{a}_i = \boldsymbol{a}(x_i)$, and $\sigma_i = \sigma(x_i)$. The spatial derivatives are discretized using the central difference scheme instead of automatic differentiation. In practice, the potential function $\psi$ or the noise intensity $\sigma$ should be replaced by a neural network. We choose a non-symmetric double-well potential function $\psi = \frac{1}{2}x^4 - x^2 + x$ and a constant noise intensity $\sigma = 1.5$ as the ground truths. For the sake of simplicity, we assume the noise intensity is known and aim to learn the potential function from the steady-state density data (1 group data as mentioned in Example 4.2, so we use 50000 epochs to train the models in this example).

The training data $\{(f(x_{i,j}, t_1), f(x_{i,j}, t), f(x_{i,j}, t_2))\}_{i,j=1}^{N,M}$ are obtained by solving the Fokker-Planck equation (4) in a bounded domain $\Omega = [-3, 3]$ with grid size $\Delta x = 0.01$ and time step size $\Delta t = 0.001$ or estimating the density function $f$ from the SDE (3) particles. We randomly select one initial distribution $\mathcal{N}(\mu, 0.2^2)$ (the mean value $\mu$ follows a uniform distribution in domain $[-2, 2]$) and choose the snapshots at $t_1 = 19.995$, $t = 20$ and $t_2 = 20.005$ as our training data (so the observation time step size is $\delta t = 5\Delta t$), i.e., the hyperparameter $M = 1$ in the loss function (15). We artificially destroy the value of the density data at two grid points $x_1$ and $x_2$. Specifically, the density data at $x_1$ is perturbed by adding noise $\alpha\epsilon$ to the raw data ($\tilde{f}(x_1) = f(x_1) + \alpha\epsilon$), while the density data at $x_2$ is perturbed by subtracting the same value, $\alpha\epsilon$, ($\tilde{f}(x_2) = f(x_2) - \alpha\epsilon$) to ensure that the integral of the density function remains equal to one. Here, $\alpha$ represents the noise ratio, and $\epsilon$ is the maximum value of the density function over the domain. See Figure 5a for the noiseless training data and Figure 5d for the corrupted training data. In this example, the ratio is selected as $\alpha = 0.2$. The learned potential functions using the PDE-based method with noiseless and corrupted training data are shown in Figure 5b and Figure 5e respectively. The learned potential functions using the EnVarA-based method with noiseless and corrupted training data are shown in Figure 5c and Figure 5f respectively. It is not surprising that our method is more robust than the discrete version of the PDE-based approach, since our EnVarA-based method does not require computing the second derivative of the density function and our loss function is in an integral form.

11

However, it should be noticed that this is a discrete version of PINN rather than the method proposed in [9, 63] since we did not use automatic differentiation here. Moreover, we employ density data as training data instead of particle data used in [9], which provides impressive results for learning stochastic differential equation with Brownian motion or Lévy motion. It is worth mentioning that the methods proposed in [9, 63] may mitigate the impact of corrupted observations, as they defined a more robust loss function. A more comprehensive comparison is left for future work.
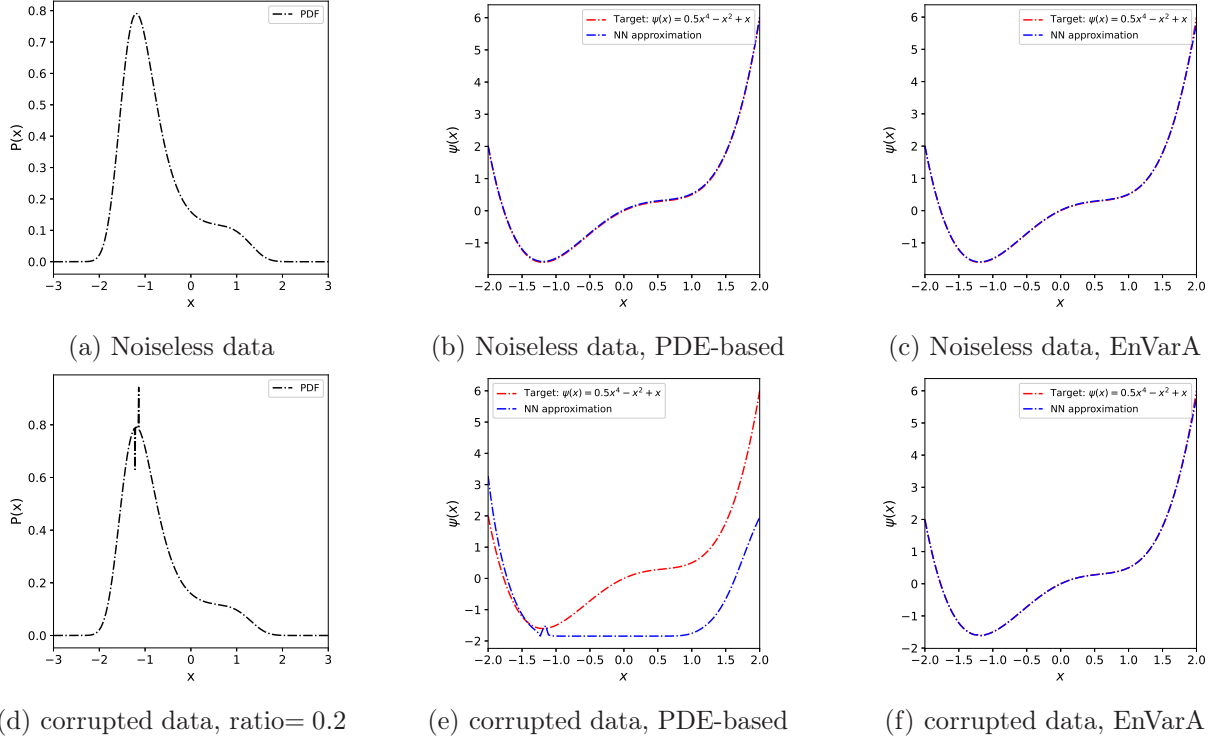


Figure 5: *(a) Noiseless training data. (b) The learned potential function $\psi_{nn}$ using noiseless training data and PDE-based method. (c) The learned potential function $\psi_{nn}$ using noiseless training data and EnVarA. (d) corrupted training data. (e) The learned potential function $\psi_{nn}$ (blue) and the G.T. $\psi$ (red) using corrupted training data and PDE-based method. (f) The learned potential function $\psi_{nn}$ (blue) and the G.T. $\psi$ (red) using corrupted training data and EnVarA.*

# 5  Discussions

We have utilized the energy-dissipation law of the underlying physical systems to derive new loss functions for learning generalized diffusions that accommodate different types of training data (density or particle data). We validated the performance of the proposed methods through several representative examples and investigated the impact of data quality and data property on these methods. Broadly speaking, our approach offers several advantages, including robustness to corrupted observations due to the weak-form of the loss function, easy extension to more general physical systems through the widely used energetic variational approach, and potential to handle higher-dimensional challenges.

One important challenge in our proposed method is handling high-dimensional problems, as

density data are not generally readily available. Instead, the density must first be approximated by particle sampling. However, estimating a high-dimensional density function is a key problem in the statistical community. Further investigation is needed to develop a more suitable loss function based directly on particle data, rather than relying on an estimated density function. These issues will be investigated in future work.

Additionally, we discuss one more alternative particle method here that is quite different from the SDE-particle based method (the particle-to-density method in Section 3.2). Instead of generating particle data with SDE (3) as described above, one can also obtain another kind of particle data that provides more information about energy dissipation.

Particles generated by both ways follow the same distribution by checking against the Fokker-Planck equation (4) and the continuity equation $f_t + \nabla \cdot (\boldsymbol{u}f) = 0$. A natural question is: what is the difference between these two groups of particles for our learning objectives?

Indeed, the particles generated by the ODE (10) not only provide distribution information, but also provide trajectory information that enable us to construct a more robust learning framework. In contrast, the particles generated by the SDE (3) can provide only distribution information so that we may construct a 'weaker' loss function as discussed in Section 3.2.

## 5.1 ODE-based particles

The general idea is to discretize the free energy using particle method. Subsequently, a learning framework can be established based on the discrete version of the energy-dissipation law.

Given particles $\{\boldsymbol{x}_i(t)\}_{i=1}^N$ (again, the number $N$ is the sample size of the distribution function) at time $t$, one can consider the empirical measure $f_N(\boldsymbol{x}, t) = \frac{1}{N} \sum_{i=1}^N \delta(\boldsymbol{x} - \boldsymbol{x}_i(t))$, where $\boldsymbol{x}_i(t)$ denotes the position of the $i$-th particle at time $t$. To approximate the term $\ln f$, we introduce a kernel function $K_h$ such that $\ln f \approx \ln f_N * K_h$, i.e.,

$$f_N * K_h(\boldsymbol{x}, t) = \int_\Omega K_h(\boldsymbol{x}, \boldsymbol{y}) f_N(\boldsymbol{y}, t) dy = \frac{1}{N} \sum_{k=1}^N K_h(\boldsymbol{x}, \boldsymbol{x}_k(t)). \tag{21}$$

In this work, we choose the kernel to be the Gaussian kernel, defined by $K_h(\boldsymbol{x}, \boldsymbol{y}) = C_h^{-1} \exp\{-\frac{\|\boldsymbol{x}-\boldsymbol{y}\|^2}{2h^2}\}$, where $C_h = (2\pi)^{\frac{d}{2}} h^d$ is the normalizing constant, $h$ is a parameter which we call it the kernel bandwidth, and $d$ is the dimension of the system (3).

Now, the discrete energy functional $E_N$ at time $t$ can be written as

$$E_N(t) = \frac{1}{N} \sum_{i=1}^N \left[ \ln \left( f_N * K_h(\boldsymbol{x}_i, t) \right) + \psi(\boldsymbol{x}_i) \right], \tag{22}$$

where we use the notation $\boldsymbol{x}_i = \boldsymbol{x}_i(t)$ for simplicity.

By checking against the ODE (10), we know that the velocity $\boldsymbol{u}$ involves the term $\nabla \ln f$ which is not well-defined at the particle level. To make sure the particles $\{\boldsymbol{x}_i(t)\}_{i=1}^N$ satisfying the energy-dissipation law at the particle level, one can derive another ODE system that approximates the original ODE (10) when $N \to \infty$. By applying EnVarA at the particle level, one can obtain the following ODE system [56]

$$\dot{\boldsymbol{x}}_i = \hat{u}_{i,N}, \tag{23}$$

13

where

$$\hat{u}_{i,N} = -\frac{\sigma^2(\boldsymbol{x}_i)}{2} \left[ \frac{\sum\limits_{j=1}^{N} \nabla_{\boldsymbol{x}_i} K_h(\boldsymbol{x}_i, \boldsymbol{x}_j)}{\sum\limits_{j=1}^{N} K_h(\boldsymbol{x}_i, \boldsymbol{x}_j)} + \sum_{k=1}^{N} \frac{\nabla_{\boldsymbol{x}_i} K_h(\boldsymbol{x}_k, \boldsymbol{x}_i)}{\sum\limits_{j=1}^{N} K_h(\boldsymbol{x}_k, \boldsymbol{x}_j)} + \nabla_{\boldsymbol{x}_i} \psi_{nn}(\boldsymbol{x}_i; \theta) \right], \quad i = 1, 2, \dots, N. \tag{24}$$

Therefore, we assume that the observation data $\{(\boldsymbol{x}_{i,j}(t_1), x_{i,j}(t), \boldsymbol{x}_{i,j}(t_2))\}_{i,j=1}^{N,M}$ are generated by this ODE system (23). Subsequently, we construct the following physics-informed loss

$$L = \sum_{j=1}^{M} \lambda(j) \left\| \frac{\boldsymbol{x}^j(t_2) - \boldsymbol{x}^j(t_1)}{t_2 - t_1} - \hat{\boldsymbol{u}}^{j,N}(t) \right\|^2, \tag{25}$$

where we use the notations $\boldsymbol{x}^j$ and $\hat{\boldsymbol{u}}^{j,N}$ to denote the vectors $\boldsymbol{x}^j = [\boldsymbol{x}_{1,j}, \boldsymbol{x}_{2,j}, \dots, \boldsymbol{x}_{N,j}]$ and $\hat{\boldsymbol{u}}^{j,N} = [\hat{\boldsymbol{u}}_{1,j,N}, \hat{\boldsymbol{u}}_{2,j,N}, \dots, \hat{\boldsymbol{u}}_{N,j,N}]$. By minimizing the loss function (25), one can find the best estimation $\psi_{nn}$.

*Remark* 5.1. Compared with the particle-to-density method, the loss function of the ODE-based method is point-wise, allowing us to bypass (at least mitigate) the ill-posed issue of the 'weak' form loss function (15). Our requirement is to be able to obtain particle data with trajectory information (ODE-based particles), which is not practical in some applications, such as cell evolution data [54]. On the other hand, the required particle information is readily available in applications such as plasma physics where particle-in-cell methods are the state-of-the-art highest fidelity solvers in high dimensions.

*Example* 5.2. **(ODE particle-based learning)**. Finally, we investigate the ODE particle-based method. The ODE (23) is derived from the discrete energy, which satisfies the energy-dissipation law in a discrete level (particle). Moreover, the ODE particle-based method is quite different from the SDE particle-based method since we can access not only the distribution information but also the trajectory information. In addition to this, the ODE-based loss function (25) is a point-wise loss function that is stronger than the energy-law based loss function (15) that is in an integral form. It is worth noting that the ODE particles are primarily generated through numerical simulations in practice.

Again, we consider the double-well system with multiplicative noise and generate particle data by solving the ODE system (23), i.e.,

$$\dot{\boldsymbol{x}}_i = -\frac{\sigma^2(\boldsymbol{x}_i)}{2} \left[ \frac{\sum\limits_{j=1}^{N} \nabla_{\boldsymbol{x}_i} K_h(\boldsymbol{x}_i, \boldsymbol{x}_j)}{\sum\limits_{j=1}^{N} K_h(\boldsymbol{x}_i, \boldsymbol{x}_j)} + \sum_{k=1}^{N} \frac{\nabla_{\boldsymbol{x}_i} K_h(\boldsymbol{x}_k, \boldsymbol{x}_i)}{\sum\limits_{j=1}^{N} K_h(\boldsymbol{x}_k, \boldsymbol{x}_j)} + \nabla_{\boldsymbol{x}_i} \psi(\boldsymbol{x}_i) \right], \quad i = 1, 2, \dots, N. \tag{26}$$

Similar to the previous examples, we simulate 20 different initial distributions $\mathcal{N}(\mu, 0.2^2)$ (the mean values $\mu$ are uniformly spaced in domain $[-2, 2]$) with time step size $\Delta t = 0.001$ and choose the snapshots at $t_1 = 0.195$, $t = 0.2$ and $t_2 = 0.205$ as our training data, where the observation time step size is chosen as $\delta t = 0.005$. Since the loss function is point-wise, we directly apply the loss to learn the potential function and the noise intensity at once. As shown in Figure 6, we can accurately learn the potential function and noise intensity. This is not surprising, as the "quality" of ODE particles is superior to that of SDE particles, allowing us to construct a point-wise loss function (25).

14
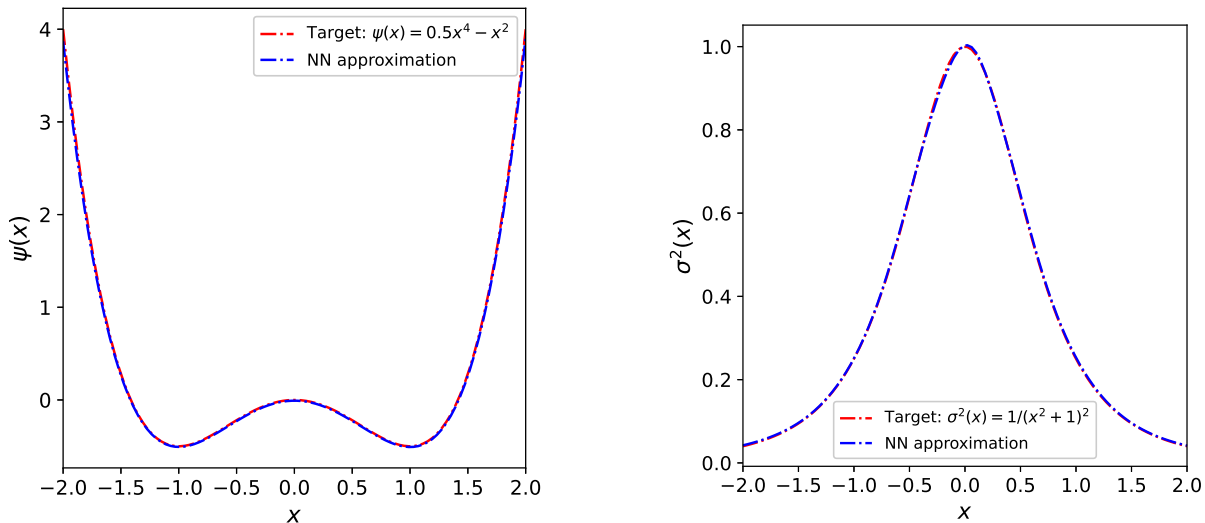
(a) Potential function. G.T.: $\psi(x) = 0.5x^4 - x^2$.

(b) Noise intensity. G.T.: $\sigma^2(x) = \frac{1}{(x^2+1)^2}$.

Figure 6: *EnVarA (ODE particle-based learning): learning potential function $\psi$ and noise intensity $\sigma^2$ at the same time.*

## Acknowledgments

## References

[1] J. Anderson, I. Kevrekidis, and R. Rico-Martinez. A comparison of recurrent training algorithms for time series analysis and system identification. *Computers & Chemical Engineering*, 20:S751–S756, 1996.

[2] V. I. Arnol'd. *Mathematical methods of classical mechanics*, volume 60. Springer Science & Business Media, 2013.

[3] T. Bertalan, F. Dietrich, I. Mezić, and I. Kevrekidis. On learning Hamiltonian systems from data. *Chaos: An Interdisciplinary Journal of Nonlinear Science*, 29(12):121107, 2019.

[4] J. Bongard and H. Lipson. Automated reverse engineering of nonlinear dynamical systems. *Proceedings of the National Academy of Sciences*, 104(24):9943–9948, 2007.

[5] S. Brunton, J. Proctor, and J. Kutz. Discovering governing equations from data by sparse identification of nonlinear dynamical systems. *Proceedings of the National Academy of Sciences*, 113(15):3932–3937, 2016.

[6] M. Budišić, R. Mohr, and I. Mezić. Applied Koopmanisma. *Chaos: An Interdisciplinary Journal of Nonlinear Science*, 22(4):047510, 2012.

[7] J. W. Burby, Q. Tang, and R. Maulik. Fast neural poincaré maps for toroidal magnetic fields. *Plasma Physics and Controlled Fusion*, 63(2), 12 2020.

[8] R. Chen and M. Tao. Data-driven prediction of general Hamiltonian dynamics via learning exactly-symplectic maps. In *Proceedings of the 38th International Conference on Machine Learning*, 2021.

[9] X. Chen, L. Yang, J. Duan, and G. E. Karniadakis. Solving inverse stochastic problems from discrete particle observations using the fokker–planck equation and physics-informed neural networks. *SIAM Journal on Scientific Computing*, 43(3):B811–B830, 2021.

[10] Y. Chen and D. Xiu. Learning stochastic dynamical system via flow map operator. *Journal of Computational Physics*, 508:112984, 2024.

[11] Z. Chen, J. Zhang, M. Arjovsky, and L. Bottou. Symplectic recurrent neural networks. In *International Conference on Learning Representations*, 2020.

[12] V. Churchill and D. Xiu. Flow map learning for unknown dynamical systems: Overview, implementation, and benchmarks. *Journal of Machine Learning for Modeling and Computing*, 4(2):173–201, 2023.

[13] F. Dietrich, A. Makeev, G. Kevrekidis, N. Evangelou, T. Bertalan, S. Reich, and I. Kevrekidis. Learning effective stochastic differential equations from microscopic simulations: Linking stochastic numerics to deep learning. *Chaos: An Interdisciplinary Journal of Nonlinear Science*, 33(2):023121, 2023.

[14] L. Ding, W. Li, S. Osher, and W. Yin. A mean field game inverse problem. *Journal of Scientific Computing*, 92(1):7, 2022.

[15] J. Feng, C. Kulick, and S. Tang. Data-driven model selections of second-order particle dynamics via integrating gaussian processes with low-dimensional interacting structures. *Physica D: Nonlinear Phenomena*, 461:134097, 2024.

[16] M. Finzi, K. Wang, and A. Wilson. Simplifying Hamiltonian and Lagrangian neural networks via explicit constraints. In *Advances in Neural Information Processing Systems*, 2020.

[17] M.-H. Giga, A. Kirshtein, and C. Liu. Variational modeling and complex fluids. *Handbook of Mathematical Analysis in Mechanics of Viscous Fluids*, pages 1–41, 2017.

[18] R. González-García, R. Rico-Martínez, and I. Kevrekidis. Identification of distributed parameter systems: A neural net based approach. *Computers & Chemical Engineering*, 22:S965–S968, 1998.

[19] S. Greydanus, M. Dzamba, and J. Yosinski. Hamiltonian neural networks. In *Advances in Neural Information Processing Systems*, 2019.

[20] A. Gruber, M. Gunzburger, L. Ju, and Z. Wang. Energetically consistent model reduction for metriplectic systems. *Computer Methods in Applied Mechanics and Engineering*, 404:115709, 2023.

[21] A. Gruber, K. Lee, H. Lim, N. Park, and N. Trask. Efficiently parameterized neural metriplectic systems. *arXiv preprint arXiv:2405.16305*, 2024.

[22] Q. Hernández, A. Badías, D. González, F. Chinesta, and E. Cueto. Structure-preserving neural networks. *Journal of Computational Physics*, 426:109950, 2021.

[23] J. Hu, J.-P. Ortega, and D. Yin. A structure-preserving kernel method for learning hamiltonian systems. *arXiv preprint arXiv:2403.10070*, 2024.

[24] Z. Hu, C. Liu, Y. Wang, and Z. Xu. Energetic variational neural network discretizations of gradient flows. *SIAM Journal on Scientific Computing*, 46(4):A2528–A2556, 2024.

[25] S. Huang, Z. He, N. Dirr, J. Zimmer, and C. Reina. Statistical-physics-informed neural networks (stat-pinns): A machine learning strategy for coarse-graining dissipative dynamics. *Journal of the Mechanics and Physics of Solids*, page 105908, 2024.

[26] S. Huang, Z. He, and C. Reina. Variational onsager neural networks (vonns): A thermodynamics-based variational learning strategy for non-equilibrium pdes. *Journal of the Mechanics and Physics of Solids*, 163:104856, 2022.

[27] P. Jin, Z. Zhang, A. Zhu, Y. Tang, and G. Karniadakis. SympNets: Intrinsic structure-preserving symplectic networks for identifying hamiltonian systems. *Neural Networks*, 132:166–179, 2020.

[28] S. Klus, F. Nüske, S. Peitz, J.-H. Niemann, C. Clementi, and C. Schütte. Data-driven approximation of the koopman generator: Model reduction, system identification, and control. *Physica D: Nonlinear Phenomena*, 406:132416, 2020.

[29] Q. Lang and F. Lu. Learning interaction kernels in mean-field equations of first-order systems of interacting particles. *SIAM Journal on Scientific Computing*, 44(1):A260–A285, 2022.

[30] K. Lee, N. Trask, and P. Stinis. Machine learning structure preserving brackets for forecasting irreversible processes. In *Advances in Neural Information Processing Systems*, 2021.

[31] Y. Liu, Y. Chen, D. Xiu, and G. Zhang. A training-free conditional diffusion model for learning stochastic dynamical systems. *arXiv preprint arXiv:2410.03108*, 2024.

[32] F. Lu, Q. An, and Y. Yu. Nonparametric learning of kernels in nonlocal operators. *Journal of Peridynamics and Nonlocal Modeling*, 2023.

[33] F. Lu, M. Maggioni, and S. Tang. Learning interaction kernels in stochastic systems of interacting particles from multiple trajectories. *Foundations of Computational Mathematics*, 22(4):1013–1067, 2022.

[34] F. Lu, M. Zhong, S. Tang, and M. Maggioni. Nonparametric inference of interaction laws in systems of agents from trajectory data. *Proceedings of the National Academy of Sciences*, 116(29):14424–14433, 2019.

[35] Y. Lu, R. Maulik, T. Gao, F. Dietrich, I. Kevrekidis, and J. Duan. Learning the temporal evolution of multivariate densities via normalizing flows. *Chaos: An Interdisciplinary Journal of Nonlinear Science*, 32(3):033121, 2022.

[36] S. Ma, S. Liu, H. Zha, and H. Zhou. Learning stochastic behaviour from aggregate data. In M. Meila and T. Zhang, editors, *Proceedings of the 38th International Conference on Machine Learning*, volume 139 of *Proceedings of Machine Learning Research*, pages 7258–7267. PMLR, 18–24 Jul 2021.

[37] M. Mattheakis, D. Sondak, A. Dogra, and P. Protopapas. Hamiltonian neural networks for solving equations of motion. *Physical Review E*, 105:065305, 2022.

[38] D. Messenger and D. Bortz. Weak SINDy for partial differential equations. *Journal of Computational Physics*, 443:110525, 2021.

[39] D. Messenger and D. Bortz. Weak SINDy: Galerkin-based data-driven model selection. *Multiscale Modeling & Simulation*, 19(3):1474–1497, 2021.

[40] D. Messenger and D. Bortz. Learning mean-field equations from particle data using WSINDy. *Physica D: Nonlinear Phenomena*, 439:133406, 2022.

[41] D. Messenger, J. Burby, and D. Bortz. Coarse-graining Hamiltonian systems using WSINDy. *arXiv preprint arXiv:2310.05879*, 2023.

[42] J. Miller, S. Tang, M. Zhong, and M. Maggioni. Learning theory for inferring interaction kernels in second-order interacting agent systems. *Sampling Theory, Signal Processing, and Data Analysis*, 21(1):21, 2023.

[43] L. Onsager. Reciprocal relations in irreversible processes. I. *Physical Review*, 37:405–426, 1931.

[44] L. Onsager. Reciprocal relations in irreversible processes. II. *Physical Review*, 38:2265–2279, 1931.

[45] M. Opper. Variational inference for stochastic differential equations. *Annalen der Physik*, 531(3):1800233, 2019.

[46] G. Papamakarios, E. Nalisnick, D. J. Rezende, S. Mohamed, and B. Lakshminarayanan. Normalizing flows for probabilistic modeling and inference. *arXiv preprint arXiv:1912.02762v1*, 2019.

[47] E. Parzen. On Estimation of a Probability Density Function and Mode. *The Annals of Mathematical Statistics*, 33(3):1065–1076, 1962.

[48] M. Raissi, P. Perdikaris, and G. Karniadakis. Physics-informed neural networks: A deep learning framework for solving forward and inverse problems involving nonlinear partial differential equations. *Journal of Computational Physics*, 378:686–707, 2019.

[49] D. J. Rezende and S. Mohamed. Variational inference with normalizing flows. *arXiv preprint arXiv:1505.05770v6*, 2016.

[50] R. Rico-Martinez, J. Anderson, and I. Kevrekidis. Continuous-time nonlinear signal processing: a neural network based approach for gray box identification. In *Proceedings of IEEE Workshop on Neural Networks for Signal Processing*, pages 596–605, 1994.

[51] M. Rosenblatt. Remarks on Some Nonparametric Estimates of a Density Function. *The Annals of Mathematical Statistics*, 27(3):832–837, 1956.

[52] H. Schaeffer. Learning partial differential equations via data discovery and sparse optimization. *Proceedings of the Royal Society A: Mathematical, Physical and Engineering Sciences*, 473(2197):20160446, 2017.

[53] M. Schmidt and H. Lipson. Distilling free-form natural laws from experimental data. *science*, 324(5923):81–85, 2009.

[54] Y. Sha, Y. Qiu, P. Zhou, and Q. Nie. Reconstructing growth and dynamic trajectories from single-cell transcriptomics data. *Nature Machine Intelligence*, 6(1):25–39, Jan 2024.

[55] J. W. Strutt. Some general theorems relating to vibrations. *Proceedings of the London Mathematical Society*, s1-4(1):357–368, 1871.

[56] Y. Wang, J. Chen, C. Liu, and L. Kang. Particle-based energetic variational inference. *Statistics and Computing*, 31(3):34, Apr 2021.

[57] Y. Wang and C. Liu. Some recent advances in energetic variational approaches. *Entropy*, 24(5), 2022.

[58] Y. Wang and C. Liu. Some recent advances in energetic variational approaches. *Entropy*, 24(5):721, 2022.

[59] M. Williams, I. Kevrekidis, and C. Rowley. A data–driven approximation of the Koopman operator: Extending dynamic mode decomposition. *Journal of Nonlinear Science*, 25(6):1307–1346, 2015.

[60] L. Yang, X. Sun, B. Hamzi, H. Owhadi, and N. Xie. Learning dynamical systems from data: A simple cross-validation perspective, part V: Sparse kernel flows for 132 chaotic dynamical systems. *Physica D: Nonlinear Phenomena*, 460:134070, 2024.

[61] H. Yu, X. Tian, W. E, and Q. Li. Onsagernet: Learning stable and interpretable dynamics using a generalized onsager principle. *Phys. Rev. Fluids*, 6:114402, 2021.

[62] J. Zhang, S. Zhang, J. Shen, and G. Lin. Energy-dissipative evolutionary deep operator neural networks. *Journal of Computational Physics*, 498:112638, 2024.

[63] R. Z. Zhang, X. Xie, and J. S. Lowengrub. Bilo: Bilevel local operator learning for pde inverse problems. *arXiv preprint arXiv:2404.17789*, 2024.

[64] Z. Zhang, Y. Shin, and G. Em Karniadakis. Gfinns: Generic formalism informed neural networks for deterministic and stochastic dynamical systems. *Philosophical Transactions of the Royal Society A*, 380(2229):20210207, 2022.